

ers that are complementary to sequences upstream and downstream of the *murA* locus and that also carry Kpn I and Xba I restriction sites (17). The *murA*, *murA^{rat1}*, and *murA^{rat2}* amplification products were double-digested with Kpn I and Xba I, and cloned into the same sites in pZE12-luc, resulting in pZE12-murA, pZE12-rat1, and pZE12-rat2, respectively. pZE12-luc is a ColE1 replicon conferring Amp^r with the luciferase reporter gene *luc* under the IPTG-inducible hybrid P_{lacO-1} promoter (24). The constructs pZA31-murA and pZA31-murA^{rat1} were constructed similarly, except that the parental vector is a p15A replicon carrying Cam^r (24). All constructs were confirmed by DNA sequencing (17).

10. T. Bernhardt, I. Wang, D. Struck, R. Young, data not shown.

11. Supplemental data, details of methods, and a figure showing the location of the altered residue on the structure of MurA are available on Science Online at www.sciencemag.org/cgi/content/full/292/5525/2326/DC1.

12. ET505 cells carrying either the A₂ plasmid (pA2) (25) or the vector (pJFlacZK) were grown in LBKan to an A₅₅₀ of 0.8 and induced with IPTG at t = 0. Immediately before induction, MgCl₂ was added to a final concentration of 0.1 M to stabilize lysing cells (4). At t = 45 min, the cells were harvested, and total sugar nucleotides were extracted and purified through a Sephadex G-25 column as described (5). The N-acetylsugar-containing fractions were pooled and further fractionated on a 1-ml Hi-Trap Source Q anion-exchange column (Pharmacia) with a 0 to 0.4 M gradient of NH₄HCO₃. To determine the major sugars present in individual peaks from the ion-exchange column, we pooled the appropriate fractions, lyophilized them, and subjected them to hydrolysis with 0.02 N HCl at 90°C for 20 min. The hydrolysate was analyzed by paper chromatography with butanol:pyridine:water (6:4:3) as the solvent system. Dried paper chromatograms were stained with alkaline silver nitrate to detect reducing sugars or with the Elson-Morgan reagent to detect aminoglycosides (26).

13. J. L. Marquardt, D. A. Siegle, R. Kolter, C. T. Walsh. *J. Bacteriol.* **174**, 5748 (1992).

14. MurA and MurA^{rat1} extracts were prepared from cultures of BL21(DE3) *slyD1 zhd::Tn10* containing the plasmids pZA31-murA and pZA31-murA^{rat1}, respectively. (The host contains the T7 gene 1, but neither plasmid contains a promoter for T7 RNA polymerase.) The cultures (35 ml) were induced with 1 mM IPTG at an A₅₅₀ of 0.2, grown for 2.5 hours (final A₅₅₀ of 2), and harvested by centrifugation (5000 rpm for 5 min in a JA20 rotor). The cells were washed with 30 ml of 50 mM tris (pH 8), resuspended in 1 ml of 50 mM tris (pH 8.0), 5 mM dithiothreitol, and disrupted in a SLM-Aminco French pressure cell at 16,000 psi. The extracts were cleared of whole cells and cell debris by centrifugation at maximum speed in a microcentrifuge for 10 min at 4°C. MurA activity was monitored as UDP-GlcNAc-dependent release of P_i from PEP as described by Marquardt *et al.* (13). Reaction mixtures contained 5 μl of 1 M tris (pH 8.0), 5 μl 10 mM UDP-GlcNAc, 5 μl of 10 mM PEP, 30 μl of buffer A [50 mM tris (pH 8.0), 100 mM NaCl, 5 mM EDTA] or 30 μl of purified Qβ phage in buffer A (30 μg of purified particles), and 5 μl of diluted MurA or MurA^{rat1} extract (2 μg of total protein). Qβ particles were purified exactly as described by Strauss and Sinsheimer (27). The phage preparation was free of contaminating proteins as judged by SDS-polyacrylamide gel electrophoresis followed by Coomassie blue staining. The resulting preparation had a viable titer of 10¹³ PFU/ml and a physical titer of 10¹⁴ particles/ml determined from a protein concentration of 1 mg/ml.

15. T. G. Bernhardt, unpublished data.

16. M. Kozak, D. Nathans, *Nature New Biol.* **234**, 209(1971).

17. W. Paranchych, in *RNA Phages*, N. D. Zinder, Ed. (Cold Spring Harbor Laboratory, Cold Spring Harbor, NY, 1975), chap. 4.

18. I.-N. Wang, R. Young, unpublished data.

19. W. Roof, R. Young, unpublished data.

20. R. B. Winter, L. Gold, *Cell* **33**, 877 (1983).

21. M. Singer *et al.*, *Microbiol. Rev.* **53**, 1 (1989).

22. J. H. Miller, *Experiments in Molecular Genetics* (Cold Spring Harbor Laboratory, Cold Spring Harbor, NY, 1972).

23. M. Sektas, M. Gregorowicz, W. Szybalski, *BioTechniques* **27**, 911 (1999).

24. R. Lutz, H. Bujard, *Nucleic Acids Res.* **25**, 1203 (1997).

25. ET505 is *E. coli* W3110 *lysA::Tn10*, obtained from the *E. coli* Genetic Stock Center (New Haven, CT; <http://cgsc.biology.yale.edu/>). A *lysA* strain is required to prevent the conversion of added [³H]DAP to lysine, so that [³H]DAP can be incorporated only into the cell wall and its precursors. The plasmid pA2 is a derivative of pJFlacZK (5) and contains the A₂ gene and the *lacZ* gene in tandem, under control of the IPTG-inducible *tac* promoter.

26. M. F. Chaplin, in *Carbohydrate Analysis: A Practical Approach*, M. F. Chaplin, J. F. Kennedy, Eds. (IRL, Oxford, 1986).

27. J. H. Strauss, R. L. Sinsheimer, *J. Mol. Biol.* **7**, 43 (1963).

28. J. van Duin, in *The Bacteriophages*, R. Calendar, Ed. (Plenum, New York, 1988), vol. 1, chap. 4.

29. N. Nannings, *Microbiol. Mol. Biol. Rev.* **62**, 110 (1998).

30. J. van Heijenoort, in *Escherichia coli and Salmonella Cellular and Molecular Biology*, F. Neidhardt, Ed. (American Society for Microbiology, Washington, DC, 1996), vol. 1, chap. 68.

31. Isogenic *murA⁺* and *murA^{rat1}* transductants of XL1 Blue *zhc-3168::Tn10kan*, constructed by P1 transduction with the original *rat1* mutant as donor, were grown to an A₅₅₀ of 0.2 at 37°C and infected at an MOI of 5 with Qβ. One milliliter of culture was withdrawn, vortexed with 1% CHCl₃, and chilled on ice at the times indicated. To estimate total Qβ production, the sample, diluted with 3 ml of LB, was subjected to disruption in a French pressure cell at 16,000 psi and then titered by plating serial dilutions on XL1 Blue.

32. We thank the members of the Young laboratory for encouragement, advice, and helpful discussion. Supported by the National Institute of General Medical Sciences (NIH), the Robert A. Welch Foundation, and the Texas Agricultural Experiment Station.

14 December 2001; accepted 12 April 2001

The Human Nuclear Xenobiotic Receptor PXR: Structural Determinants of Directed Promiscuity

Ryan E. Watkins,¹ G. Bruce Wisely,³ Linda B. Moore,³ Jon L. Collins,³ Millard H. Lambert,³ Shawn P. Williams,³ Timothy M. Willson,³ Steven A. Kliewer,³ Matthew R. Redinbo^{2*}

The human nuclear pregnane X receptor (hPXR) activates cytochrome P450-3A expression in response to a wide variety of xenobiotics and plays a critical role in mediating dangerous drug-drug interactions. We present the crystal structures of the ligand-binding domain of hPXR both alone and in complex with the cholesterol-lowering drug SR12813 at resolutions of 2.5 and 2.75 angstroms, respectively. The hydrophobic ligand-binding cavity of hPXR contains a small number of polar residues, permitting SR12813 to bind in three distinct orientations. The position and nature of these polar residues were found to be critical for establishing the precise pharmacologic activation profile of PXR. Our findings provide important insights into how hPXR detects xenobiotics and may prove useful in predicting and avoiding drug-drug interactions.

The pregnane X receptor (PXR; also known as NR1I2), a member of the nuclear receptor family of ligand-activated transcription factors, is a key regulator of cytochrome P450-3A (*CYP3A*) gene expression in mammalian liver and small intestine (1–5). The *CYP3A* gene products are heme-containing proteins that metabolize a wide variety of chemicals, including >50% of all prescription drugs (6). PXR is activated by most of the xenobiotics (exogenous chemicals)

that are known to induce *CYP3A* gene expression, including the commonly used antibiotic rifampicin, the glucocorticoid dexamethasone, and the herbal antidepressant St. John's wort (1–4, 7, 8). Like other nuclear receptors, PXR contains both a DNA-binding domain and a ligand-binding domain. PXR binds to the xenobiotic DNA response elements in the regulatory regions of *CYP3A* genes as a heterodimer with the 9-cis retinoic acid receptor, also known as the retinoid X receptor (RXR) (1, 2, 4).

PXR can mediate dangerous drug-drug interactions. For example, hyperforin, a constituent of St. John's wort, activates PXR and up-regulates *CYP3A* expression, which leads to the metabolism of vital drugs including the antiretroviral drug indinavir and the immunosuppressant compound cyclosporin (8–11). Unlike the steroid, retinoid, and thyroid hormone recep-

¹Department of Biochemistry and Biophysics, School of Medicine, ²Department of Chemistry and Lineberger Comprehensive Cancer Center, University of North Carolina (UNC) at Chapel Hill, Chapel Hill, NC 27599, USA. ³Nuclear Receptor Discovery Research, GlaxoSmithKline, Research Triangle Park, NC 27709, USA.

*To whom correspondence should be addressed. E-mail: redinbo@unc.edu

REPORTS

tors, which are highly selective for their cognate hormone, PXR has evolved to detect structurally diverse compounds. These include exogenous drugs and toxins as well as endogenous compounds, such as lithocholic acid (a toxic bile acid) and certain C21 steroids (pregnanes) (1, 3, 7). Although these diverse interactions imply promiscuity, PXR also exhibits specificity, as evidenced by the differences in the pharmacologic activation profile of PXR across species. For instance, human PXR is activated by rifampicin and the cholesterol-lowering drug SR12813 (12, 13), whereas mouse PXR is not (7); mouse PXR is activated by the synthetic steroid 5-pregnen-3 β -ol-20-one-16 α -carbonylnitrile (PCN), whereas the human receptor is not. Thus, by binding diverse but precise arrays of compounds, PXR exhibits directed promiscuity.

Unraveling the structural basis of how PXR recognizes an array of different endogenous and exogenous compounds is critical to our understanding of how harmful compounds are cleared from the body and may also improve our ability to predict and avoid dangerous drug-drug interactions. Accordingly, two structures of the ligand-binding domain of hPXR (hPXR-

LBD) were determined by molecular replacement (14) and were refined with the program CNS (15): an apo structure at 2.5 Å resolution, and a complex with the high-affinity ligand SR12813 (dissociation constant $K_d = 41$ nM) at 2.75 Å resolution (Table 1).

The hPXR-LBD is an “ α -helical sandwich” composed of three layers: $\alpha 1/\alpha 3$, $\alpha 4/\alpha 5/\alpha 8$, and $\alpha 7/\alpha 10$. This region of the molecule is similar to nuclear receptor LBDs of known structure (16, 17) (Fig. 1A). The standard three-stranded β sheet is expanded to a five-stranded antiparallel β sheet (Fig. 1B), and the ligand-binding cavity is localized at the bottom of the molecule. The structures of the apo and ligand-bound forms of the hPXR-LBD are similar, exhibiting a root mean square deviation (RMSD) of 0.89 Å over all atoms. In both the apo and SR12813-bound structures, the activation function 2 helix (α AF), which plays a critical role in transcriptional activation, is packed against the body of the receptor in a position that appears permissive for coactivator interactions. The hPXR-LBD is most closely related in structure to the vitamin D receptor (VDR) (18), sharing 45% sequence identity and 1.8 Å

RMSD over 225 equivalent C α positions. More limited structural similarity (2.4 to 2.9 Å RMSD) is shared with RXR, peroxisome proliferator-activated receptor γ (PPAR γ), and the estrogen and progesterone receptors (19–24) [Web table 1 and Web fig. 1 (25)].

Although the hPXR-LBD is similar to known nuclear receptor LBDs, it contains several distinct features that appear critical to its function as a promiscuous xenobiotic receptor. First, the variable region between $\alpha 1$ and $\alpha 3$ is a four-residue turn in the hPXR-LBD (Fig. 1A). In the PPARs, this region contains $\alpha 2$ and is the proposed ligand access site for the binding pocket (21, 26). Second, $\alpha 6$ is replaced in the hPXR-LBD by a conserved, flexible loop (residues 309 to 321) that lies adjacent in space to the ligand-binding cavity and may be involved in accommodation of both small and large ligands in the binding pocket. Third, the hPXR-LBD has two additional β strands not observed previously in a nuclear receptor LBD (Fig. 1A) (17). These form the fourth ($\beta 1$, residues 210 to 217) and fifth ($\beta 1'$, residues 221 to 226) strands of a five-stranded antiparallel β sheet (Fig. 1B). An “insertion domain” containing roughly the same number of residues (but only 12% se-

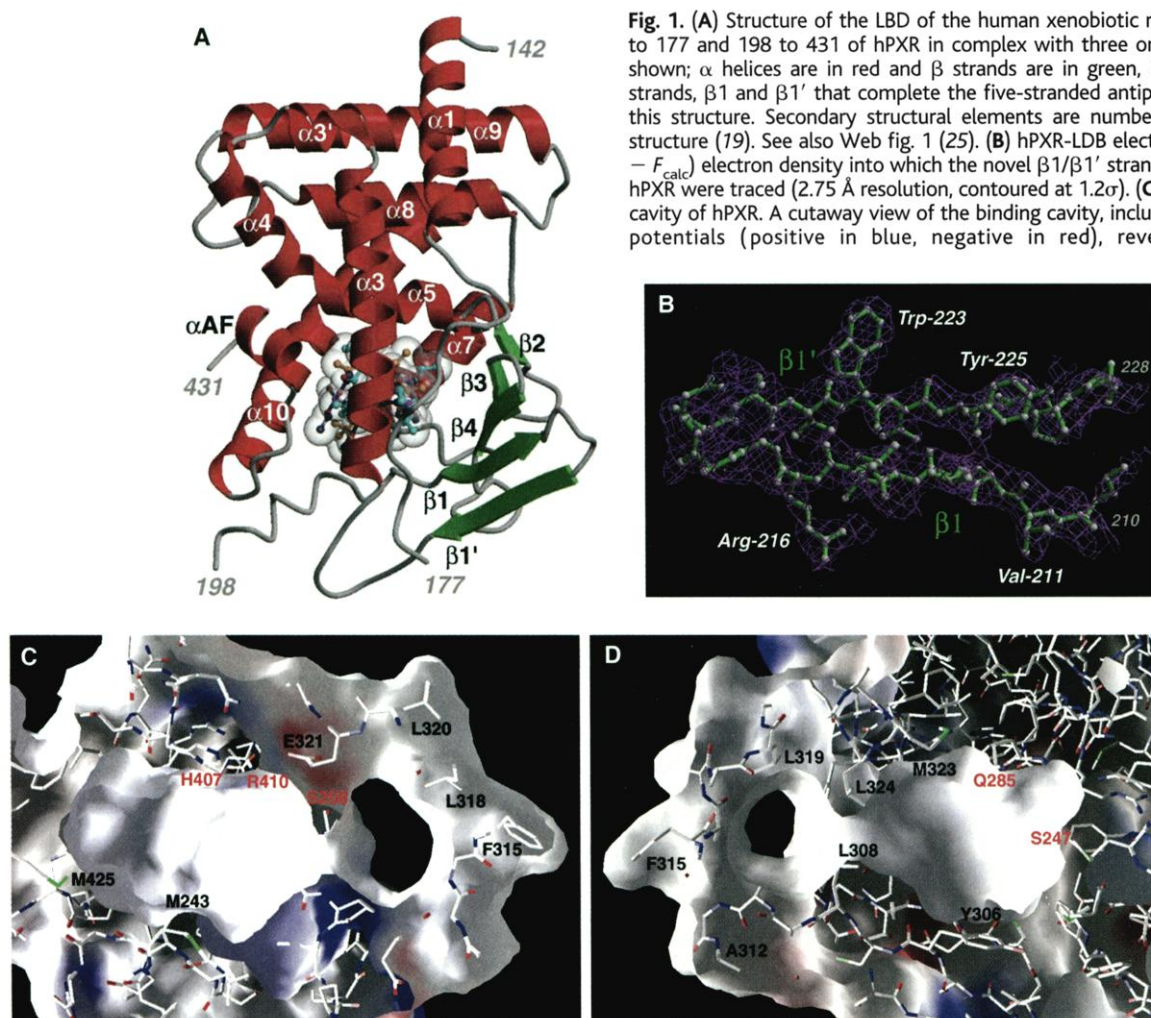


Fig. 1. (A) Structure of the LBD of the human xenobiotic receptor PXR. Residues 142 to 177 and 198 to 431 of hPXR in complex with three orientations of SR12813 are shown; α helices are in red and β strands are in green, including the two novel β strands, $\beta 1$ and $\beta 1'$ that complete the five-stranded antiparallel β sheet observed in this structure. Secondary structural elements are numbered according to the RXR structure (19). See also Web fig. 1 (25). (B) hPXR-LBD electron density: unbiased ($F_{\text{obs}} - F_{\text{calc}}$) electron density into which the novel $\beta 1/\beta 1'$ strands (residues 210 to 228) of hPXR were traced (2.75 Å resolution, contoured at 1.2σ). (C and D) The ligand-binding cavity of hPXR. A cutaway view of the binding cavity, including electrostatic surface potentials (positive in blue, negative in red), reveals a relatively smooth, uncharged surface. The cavity is enclosed by portions of five α helices ($\alpha 3$, $\alpha 5$, $\alpha 7$, $\alpha 10$, and α AF), three β strands ($\beta 1$, $\beta 3$, and $\beta 4$), and three loops (the $\alpha 10$ - α AF region and the two mobile regions between $\beta 4$ and $\alpha 7$ and from residue 198 to $\beta 1$). Select residues lining the cavity are indicated. In particular, the positions of the following polar residues that contact SR12813 are indicated in red: Ser²⁰⁸, Ser²⁴⁷, Gln²⁸⁵, His⁴⁰⁷, and Arg⁴¹⁰. Regions of the surface 309–321 loop, which may facilitate the expansion of the ligand-binding pocket, are also shown, including the conserved hydrophobic residues Phe³¹⁵, Leu³¹⁸, Leu³¹⁹, and Leu³²⁰.

quence identity) was engineered out of the VDR before crystallization and structure determination (18) [Web fig. 1 (25)].

The ligand-binding cavity of the hPXR-LBD is largely hydrophobic and is lined by 28 amino acid residues that are desolvated when SR12813 binds. The structures of the apo and

ligand-bound cavities are similar, exhibiting a RMSD of 1.12 Å over all atoms in the 28 residues. The binding cavity volume of 1150 Å³ is substantially larger than that of many other nuclear receptors, including the progesterone, estrogen, retinoid, and thyroid hormone receptors. Twenty cavity-lining residues are hydrophobic, four are polar (Ser²⁰⁸, Ser²⁴⁷, Cys²⁸⁴, and Gln²⁸⁵), and four are charged or potentially charged (Glu³²¹, His³²⁷, His⁴⁰⁷, and Arg⁴¹⁰) [Web table 2 (25)]. A salt bridge between Glu³²¹ and Arg⁴¹⁰ effectively neutralizes their charged character, so that the inner surface of this ligand-binding cavity is relatively uncharged and hydrophobic (Fig. 1, C and D). Five critical polar residues spaced evenly throughout the upper portion of the ligand-binding cavity form key binding interactions with SR12813 (Ser²⁰⁸, Ser²⁴⁷, Gln²⁸⁵, His⁴⁰⁷, and Arg⁴¹⁰) (Fig. 1, C and D).

hPXR is able to bind both small and large ligands. The flexible loop involving residues 309 to 321 spans the space between the COOH-terminus of β4 and the NH₂-terminus of α7, and exhibits a mean thermal displacement parameter of 82.3 Å² over main-chain atoms despite persistent electron density. Nine of the 13 residues in this loop are completely conserved in the mammalian PXR molecules of known sequence, including four solvent-exposed hydrophobic residues (Phe³¹⁵, Leu³¹⁸, Leu³¹⁹, and Leu³²⁰). The 309–321 loop is linked to the ligand-binding cavity of hPXR by a non-solvent-accessible pore (Fig. 1, C and D). The binding of a large compound (e.g., rifampicin) may force this pore to open, lining an enlarged ligand-binding pocket with additional hydrophobic residues. Thus, structural flexibility may allow PXR to bind both to small ligands and to the much larger compound rifampicin.

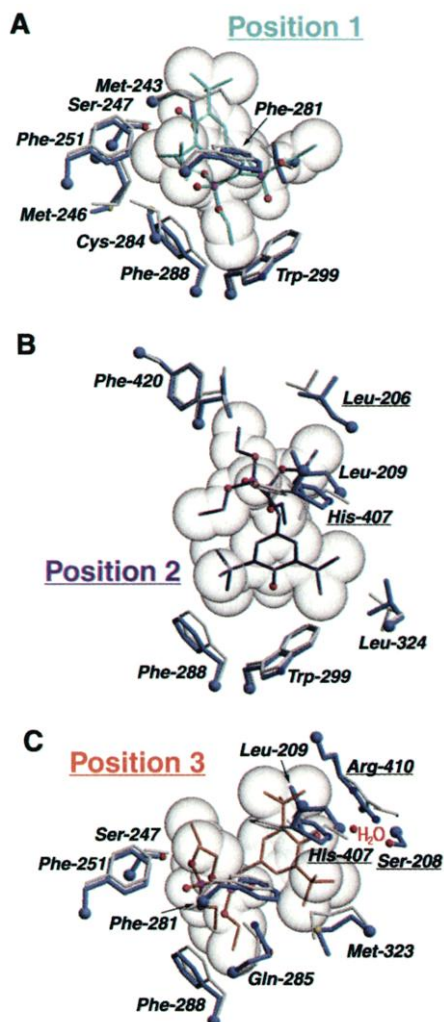


Fig. 2. Three experimentally observed positions of SR12813 in the ligand-binding pocket of hPXR. Intermolecular interactions are shown with amino acid side chains in blue and the C α atom as a sphere. The positions 1, 2, and 3 of SR12813 are rendered in cyan, purple, and orange, respectively. Equivalent side chains from the apo structure are shown in white. A small number of residues undergo rotamer shifts (Met²⁴³, Cys²⁸⁴, and His⁴⁰⁷) or small shifts in position (Ser²⁰⁸ and Leu²⁰⁹) upon SR12813 binding. Residues mutated to examine the specificity of mouse PXR are underlined. (A) Position 1 makes van der Waals contacts with eight side chains, and forms one 3.0 Å hydrogen bond with Ser²⁴⁷. (B) Position 2 makes van der Waals contacts with seven side chains, and forms one 2.8 Å hydrogen bond with His⁴⁰⁷. (C) Position 3 makes van der Waals contacts with six side chains, and forms three hydrogen bonds with Ser²⁴⁷, Gln²⁸⁵, and Ser²⁰⁸, which forms a water-mediated hydrogen bond. See also Web table 2 and Web fig. 2 (25).

Table 1. Crystallographic data and refinement statistics. Data from crystals containing l-SR12813 were used only to guide and confirm the positioning of SR12813 ligands; thus, a refined structure was not generated. Crystallization: The purified hPXR-LBD/SRC-1 complex (30) was concentrated in 250 mM NaCl, 20 mM tris-HCl (pH 7.8), 5% glycerol (v/v), 5 mM dithiothreitol, and 2.5 mM EDTA in the presence of 10-fold molar excesses of the SR12813 or l-SR12813 compounds to final concentrations of 4 and 5 mg/ml, respectively. SR12813 and l-SR12813 were synthesized in-house. The apo complex was concentrated in the same buffer to 5 mg/ml. Crystallization of hPXR-LBD was achieved by hanging-drop vapor diffusion at 22°C against the following condition: 50 mM imidazole at pH 7.2, 10% 2-propanol. The purified hPXR-LBD protein used in the crystallography (comprising residues 130 to 434) was in a 1:1 complex with amino acids 623 to 710 of the human transcriptional coactivator protein SRC-1 (31). However, this 88-amino acid coactivator peptide was not observed bound to PXR in the structure, and examination of extensively washed and dissolved crystals by SDS-PAGE revealed that this coactivator fragment was not present. Structure determination: Structures were determined by molecular replacement with AMoRe (14) using the crystal structure of the VDR as a search model (45% sequence identity over 225 equivalent C α positions). Clear solutions were obtained in the proper enantiomorphic space group, P₄₃2₁2. The asymmetric unit contains one hPXR-LBD monomer. The structures were refined using torsion angle dynamics in CNS with the maximum likelihood function target, and included an overall anisotropic B factor and a bulk solvent correction (15). Residues 142 to 177 and 198 to 431 of hPXR-LBD were traced in the structures reported here. Ordered electron density for the remaining amino acids was not observed at any time during refinement. For both structures, 10% of the observed data were set aside for cross-validation using the R_{free} statistic before any structural refinement (32). Manual adjustments and rebuilding of the model were performed using the program O (33) and sigmaA-weighted electron density maps (34). At the later stages of refinement, 281 and 166 solvent sites were added to the apo and SR12813 complexes, respectively. Structures exhibit good geometry with no Ramachandran outliers. Molecular graphics figures were created with MOLSCRIPT (35), Raster-3D (36), and Grasp (37).

	APO	SR12813	l-SR12813
Resolution (Å; highest shell)	20–2.5 (2.54–2.5)	20–2.75 (2.8–2.75)	20–3.0 (3.05–3.0)
Space group	P ₄ ₃ 2 ₁ 2	P ₄ ₃ 2 ₁ 2	P ₄ ₃ 2 ₁ 2
Cell constants (Å)	a = 91.6; c = 85.0	a = 91.3; c = 85.3	a = 91.1; c = 84.5
Total reflections	179,671	133,315	91,752
Unique reflections	12,611	9,512	7,269
Mean redundancy	14.2	14	12.6
R _{sym} * (%; highest shell)	7.3 (39.0)	9.8 (40.0)	9.7 (51.0)
Completeness (%; highest shell)	99.9 (100)	99.6 (100)	99.9 (100)
Mean I/σ (highest shell)	40.8 (7.9)	25.9 (3.7)	31.4 (5.4)
R _{cryst} † (%; highest shell)	20.9 (25.9)	21.3 (26.1)	—
R _{free} ‡ (%; highest shell)	28.4 (32.1)	27.4 (40.5)	—
RMSD bond lengths (Å)	0.0059	0.0093	—
RMSD bond angles (°)	1.11	1.29	—
RMSD dihedrals (°)	20.54	21.33	—
RMSD impropers (°)	0.71	0.91	—
Number protein atoms	2,141	2,141	—
Number solvent sites	281	166	—
Number ligand atoms	—	99	—

*R_{sym} = Σ|I - ⟨I⟩|/ΣI, where I is the observed intensity and ⟨I⟩ is the average intensity of multiple symmetry-related observations of that reflection. †R_{cryst} = Σ||F_{obs}| - |F_{calc}||/Σ|F_{obs}|, where F_{obs} and F_{calc} are the observed and calculated structure factors, respectively. ‡R_{free} = Σ||F_{obs}| - |F_{calc}||/Σ|F_{obs}| for 10% of the data not used at any stage of structural refinement.

Three distinct binding modes of the high-affinity ligand SR12813 (positions 1, 2, and 3) were observed in the ligand-binding cavity of hPXR (Fig. 2). These orientations were identified during structural refinement and were rigorously confirmed using difference maps involving data obtained from crystals containing an iodinated form of SR12813 (I-SR12813) (27). Each orientation forms distinct interactions with residues that line the ligand-binding cavity of PXR. Although ligand position 3 forms the most hydrophilic interactions, positions 1 and 2 were clearly indicated in the detailed examination of difference maps and in refinement. Of the 19 residues involved in contacting these orientations of SR12813, only Phe²⁸⁸ interacts with all three ligand conformations; a phenylalanine residue is conserved at position 288 in the known mammalian PXR sequences. The remainder of the hydrophobic residues contact either one or two ligand orientations (Fig. 2). Two polar side chains (Ser²⁴⁷ and His⁴⁰⁷) interact with two orientations of the ligand; the remaining four (Ser²⁰⁸, Cys²⁸⁴, Gln²⁸⁵, and Arg⁴¹⁰) interact with only one orientation [Web table 2 and Web fig. 2 (25)].

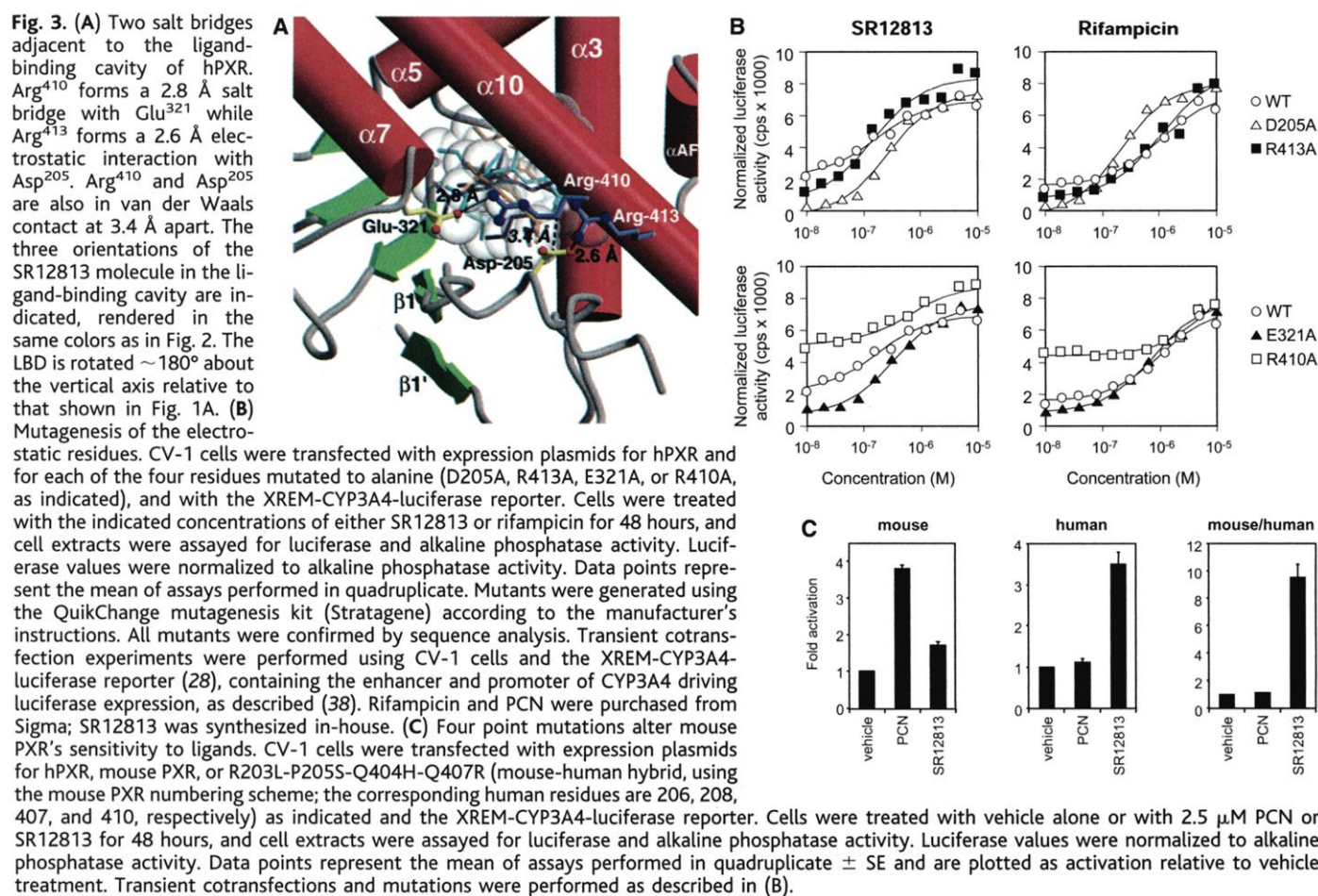
Two salt bridges occur across the region of the ligand-binding cavity that is closest to the surface of hPXR: Arg⁴¹⁰-Glu³²¹ and Arg⁴¹³-Asp²⁰⁵ (Fig. 3A). To examine the functional

relevance of these salt bridges, we individually mutated each of these residues to alanine. Using a luciferase reporter gene assay (28), we treated CV-1 cells with increasing concentrations of either SR12813 or rifampicin (Fig. 3B). Mutation of Asp²⁰⁵ resulted in a marked decrease in the basal (ligand-independent) transcriptional activity of PXR, whereas mutation of either Glu³²¹ or Arg⁴¹³ modestly reduced PXR basal activity. In contrast, changing Arg⁴¹⁰ resulted in a marked increase in the basal activity of PXR. These data demonstrate the importance of these residues in determining the basal activity of the PXR. In addition, rifampicin was found to be a more potent activator of Asp²⁰⁵ → Ala PXR than of wild-type PXR. This effect was not seen with SR12813, which suggests that SR12813 and rifampicin bind to PXR in different ways.

Marked differences in the pharmacological activation profiles of PXR occur across species. For example, human and rabbit PXR are activated efficiently by SR12813, whereas mouse PXR is not. Conversely, mouse PXR is activated more efficiently by the synthetic steroid PCN than by the human or rabbit orthologs (7, 29). We next investigated the importance of the polar residues in the pocket in establishing these species differences. Four residues that interact with SR12813 in the hPXR crystal structure and differ between human and mouse

PXR were chosen for mutagenesis (Fig. 2) [Web table 2 (25)]. Each of these residues was mutated in the context of a mouse PXR expression plasmid to the corresponding hPXR amino acid: Arg²⁰³ → Leu, Pro²⁰⁵ → Ser, Gln⁴⁰⁴ → His, and Gln⁴⁰⁷ → Arg (R203L-P205S-Q404H-Q407R), using the mouse numbering scheme. As expected, wild-type mouse PXR responded to PCN and was only weakly activated by SR12813 in reporter assays (Fig. 3C). However, the R203L-P205S-Q404H-Q407R mutant (mouse-human hybrid PXR) was no longer activated by PCN but was activated efficiently by SR12813. Thus, by using the crystal structure to design targeted mutants, we were able to confer a human-like response to the mouse PXR. This finding indicates that PXR selectivity can be affected by changes in only a few polar residues within the molecule's ligand-binding cavity.

In summary, the hPXR-LBD has evolved several structural features that permit it to function as a broad chemical "sensor." A small number of polar residues are spaced throughout the smooth, hydrophobic ligand-binding pocket of hPXR. Changes in only a few of these polar residues can have marked effects on the responsiveness of hPXR to various xenobiotics. The character of the ligand pocket mirrors the character of most of the known PXR ligands, which



are generally hydrophobic and contain a small number of polar groups capable of hydrogen bonding. The unique composition of the ligand pocket not only allows hPXR to bind a diverse set of chemicals, but also (as seen with SR12813) permits a single ligand to dock in multiple orientations. This binding mode stands in sharp contrast to other nuclear receptor–ligand interactions, which have evolved to be highly specific. Because hPXR activation is responsible for an important class of drug–drug interactions, these structures may be useful for in silico screening of drug candidates to predict and avoid dangerous side effects.

References and Notes

1. S. A. Klierer *et al.*, *Cell* **92**, 73 (1998).
2. J. M. Lehmann *et al.*, *J. Clin. Invest.* **102**, 1016 (1998).
3. G. Bertilsson *et al.*, *Proc. Natl. Acad. Sci. U.S.A.* **95**, 12208 (1998).
4. B. Blumberg *et al.*, *Genes Dev.* **12**, 3195 (1998).
5. W. Xie *et al.*, *Nature* **406**, 435 (2000).
6. P. Maurel, in *Cytochromes P450: Metabolic and Toxicological Aspects*, C. Ioannides, Ed. (CRC Press, Boca Raton, FL, 1996), pp. 241–270.
7. S. A. Jones *et al.*, *Mol. Endocrinol.* **14**, 27 (2000).
8. L. B. Moore *et al.*, *Proc. Natl. Acad. Sci. U.S.A.* **97**, 7500 (2000).
9. S. C. Piscitelli, A. H. Burstein, D. Chait, R. M. Alfaro, J. Falloon, *Lancet* **355**, 547 (2000).
10. F. Ruschitzka, P. J. Meier, M. Turina, T. F. Luscher, G. Noll, *Lancet* **355**, 548 (2000).
11. J. M. Wentworth, M. Agostini, J. Love, J. W. Schwabe, V. K. Chatterjee, *J. Endocrinol.* **166**, R11 (2000).
12. T. A. Berkhout *et al.*, *J. Biol. Chem.* **271**, 14376 (1996).
13. T. A. Berkhout *et al.*, *Atherosclerosis* **133**, 203 (1997).
14. J. Navaza, P. Saludjian, *Methods Enzymol.* **276A**, 581 (1997).
15. A. T. Brünger *et al.*, *Acta Crystallogr.* **D54**, 905 (1998).
16. D. Moras, H. Gronemeyer, *Curr. Opin. Cell Biol.* **10**, 384 (1998).
17. R. V. Weatherman, R. J. Fletterick, T. S. Scanlan, *Annu. Rev. Biochem.* **68**, 559 (1999).
18. N. Rochel, J. M. Wurtz, A. Mitschler, B. Klaholz, D. Moras, *Mol. Cell* **5**, 173 (2000).
19. W. Bourguet, M. Ruff, P. Chambon, H. Gronemeyer, D. Moras, *Nature* **375**, 377 (1995).
20. J.-P. Renaud *et al.*, *Nature* **378**, 681 (1995).
21. R. T. Nolte *et al.*, *Nature* **395**, 137 (1998).
22. S. P. Williams, P. B. Sigler, *Nature* **393**, 392 (1998).
23. A. K. Shiau *et al.*, *Cell* **95**, 927 (1998).
24. A. M. Brzozowski *et al.*, *Nature* **389**, 753 (1997).
25. For supplementary figures and tables, see *Science Online* (www.sciencemag.org/cgi/content/full/1060762/DC1).
26. R. T. Gampe Jr. *et al.*, *Mol. Cell* **5**, 545 (2000).
27. Placing single SR12813 molecules into the clear electron density in the PXR binding pocket resulted in adjacent positive electron density peaks, suggesting that more than one conformation of the ligand was present. This was confirmed using difference density generated from crystals of hPXR-LBD containing an iodinated form of SR12813 (I-SR12813), in which the two *t*-butyl groups of SR12813 were replaced with iodine. I-SR12813 was found to activate PXR as efficiently as did SR12813 (L. B. Moore, J. L. Collins, T. M. Willson, data not shown). Two difference density maps were used to guide positioning SR12813 ligands: $(|F_{obs}^{I-SR12813}| - |F_{obs}^{SR12813}|)$, $(\phi_{calc}^{PROTEIN})$ and $(|F_{obs}^{I-SR12813}| - |F_{calc}^{PROTEIN}|)$, $(\phi_{calc}^{PROTEIN})$, each calculated to 3.0 Å resolution (Table 1). Both maps showed a consistent set of significant positive difference density peaks (the highest peaks in both maps) in the ligand-binding pocket, which were interpreted to be the iodine atoms. Three SR12813 ligands optimally satisfied the electron density in the binding pocket: Position 1 was placed on the basis of two σ difference density

- peaks observed in both maps, position 3 on the basis of two σ difference density peaks, and position 2 on the basis of two 4σ difference density peaks. Occupancies of each ligand position were estimated on the basis of iodine difference density and standard electron density peaks, and were fixed at 0.4, 0.2, and 0.4 for positions 1, 2, and 3, respectively.
28. B. Goodwin, E. Hodgson, C. Liddle, *Mol. Pharmacol.* **56**, 1329 (1999).
29. U. Savas, M. R. Wester, K. J. Griffin, E. F. Johnson, *Drug Metab. Disp.* **28**, 529 (2000).
30. Residues 130 to 434 of hPXR-LBD were engineered as an NH₂-terminal polyhistidine-tagged fusion protein and subcloned into the pRSETA expression vector (Invitrogen). Residues 623 to 710 of the human SRC-1 protein were subcloned into the bacterial vector pACYC184 (American Type Culture Collection 37033) along with a T7 promoter (27). The hPXR-LBD–pRSETA and SRC-1–pACYC184 plasmids were cotransformed into the BL21(DE3) strain of *Escherichia coli* and expressed with isopropyl- β -D-thiogalactopyranoside in shaker flasks at 22°C. Cell pellets were resuspended, lysed by sonication, and clarified by centrifugation. The cleared supernatant was loaded onto ProBond nickel-chelating resin (Invitrogen). The PXR-LBD–SRC-1 complex was eluted using 500 mM imidazole (pH 7.5). Fractions were pooled, concentrated using Centri-prep 30K (Amicon) units, and subjected to size exclusion using Sepharose S-75 resin (Pharmacia). Column fractions containing the PXR–SRC-1 complex were pooled and loaded onto a 50-ml Mono-S Sepharose Fast Flow column (Pharmacia). The protein complex was eluted from the column at 300 mM NaCl in an increasing salt gradient. The appropriate column fractions, which contained the 1:1 PXR–SRC-1 complex, were pooled and stored on ice. Purity for the PXR–SRC-1 complex was

- estimated at >95%, as assessed by SDS–polyacrylamide gel electrophoresis (PAGE) with silver staining.
31. S. A. Onate, S. Y. Tsai, M. J. Tsai, B. W. O'Malley, *Science* **270**, 1354 (1995).
32. A. T. Brünger, *Acta Crystallogr.* **D49**, 24 (1993).
33. T. A. Jones, J. Y. Zou, S. W. Cowan, M. Kjeldgaard, *Acta Crystallogr.* **A47**, 110 (1991).
34. R. J. Read, *Acta Crystallogr.* **A42**, 140 (1986).
35. P. J. Kraulis, *J. Appl. Crystallogr.* **24**, 946 (1991).
36. E. A. Merritt, D. J. Bacon, *Methods Enzymol.* **277**, 505 (1997).
37. A. Nicholls, K. A. Sharp, B. Honig, *Proteins* **11**, 281 (1991).
38. L. B. Moore *et al.*, *J. Biol. Chem.* **275**, 15122 (2000).
39. We thank B. Bernstein and R. Thapar for critical comments on the manuscript; P. Kuhn, M. Soltis (Stanford Synchrotron Radiation Facility), A. Howard, L. Keefe (Advanced Photon Source), E. Collins, and L. Betts for assistance with data collection; J. Shenk for experimental assistance; and members of the Redinbo group, including Y. Xue, J. Chrencik, T. Thieu, S. Bencharit, and E. Howard-Williams, for experimental and data collection assistance. Supported by a Glaxo-UNC Collaborative Research Grant, the UNC Lineberger Comprehensive Cancer Center, and a Burroughs Wellcome Career Award in the Biomedical Sciences (M.R.R.). Coordinates for the apo and SR12813-bound forms of hPXR-LBD have been deposited with the Research Collaboratory for Structural Bioinformatics and assigned Protein Data Bank accession codes 1ILG and 1ILH, respectively.

16 March 2001; accepted 11 May 2001
 Published online 14 June 2001;
 10.1126/science.1060762
 Include this information when citing this paper.

Recruitment of HAT Complexes by Direct Activator Interactions with the ATM-Related Tra1 Subunit

Christine E. Brown,^{1,2} LeAnn Howe,^{1,2} Kyle Sousa,^{1,2} Stephen C. Alley,³ Michael J. Carrozza,^{1,2} Song Tan,² Jerry L. Workman^{1*}

Promoter-specific recruitment of histone acetyltransferase activity is often critical for transcriptional activation. We present a detailed study of the interaction between the histone acetyltransferase complexes SAGA and NuA4, and transcription activators. We demonstrate by affinity chromatography and photo-cross-linking label transfer that acidic activators directly interact with Tra1p, a shared subunit of SAGA and NuA4. Mutations within the COOH-terminus of Tra1p disrupted its interaction with activators and resulted in gene-specific transcriptional defects that correlated with lowered promoter-specific histone acetylation. These data demonstrate that the essential Tra1 protein serves as a common target for activators in both SAGA and NuA4 acetyltransferases.

The recruitment of histone acetyltransferase complexes to genomic loci via direct interactions with transcriptional activators

is important for the regulation of gene expression (*1*). We have previously shown that two yeast histone acetyltransferase (HAT) complexes, SAGA and NuA4, specifically interact with acidic activation domains and selectively stimulate transcription driven by these activators from chromatin templates in vitro (2–4). The 1.8-megadalton (MD) SAGA complex contains at least 14 subunits, and preferentially

¹Howard Hughes Medical Institute, ²Department of Biochemistry and Molecular Biology, ³Department of Chemistry, The Pennsylvania State University, 306 Althouse Laboratory, University Park, PA 16802, USA.

*To whom correspondence should be addressed: E-mail: jlw10@psu.edu